Negative Capacitance in a Ferroelectric Capacitor

Asif Islam Khan[1], Korok Chatterjee[1], Brian Wang[1], Steven Drapcho[2], Long You[1], Claudy Serrao[1], Saidur Rahman Bakaul[1], Ramamoorthy Ramesh[2,3,4], Sayeef Salahuddin[1,4*]

[1] Dept. of Electrical Engineering and Computer Sciences, University of California, Berkeley
[2] Dept. of Physics, University of California, Berkeley
[3] Dept. of Material Science and Engineering, University of California, Berkeley
[4] Material Science Division, Lawrence Berkeley National Laboratory, Berkeley,

*To whom correspondence should be addressed; E-mail: sayeef@berkeley.edu

The Boltzmann distribution of electrons poses a fundamental barrier to lowering energy dissipation in conventional electronics, often termed as Boltzmann Tyranny[1-5]. Negative capacitance in ferroelectric materials, which stems from the stored energy of phase transition, could provide a solution, but a direct measurement of negative capacitance has so far been elusive[1-3]. Here we report the observation of negative capacitance in a thin, epitaxial ferroelectric film. When a voltage pulse is applied, the voltage across the ferroelectric capacitor is found to be decreasing with time–in exactly the opposite direction to which voltage for a regular capacitor should change. Analysis of this 'inductance'-like behavior from a capacitor presents an unprecedented insight into the intrinsic energy profile of the ferroelectric material and could pave the way for completely new applications.

Owing to the energy barrier that forms during phase transition and separates the two degenerate polarization states, a ferroelectric material could show negative differential capacitance while in non-equilibrium[1-5]. The state of negative capacitance is unstable, but just as a series resistance can stabilize the negative differential resistance of an Esaki diode, it is also possible to stabilize a ferroelectric in the negative differential capacitance state by placing a series dielectric capacitor [1-3]. In this configuration, the ferroelectric acts as a 'transformer' that boosts up the input voltage. The resulting amplification could lower the voltage needed to operate a transistor below the limit otherwise imposed by the Boltzmann distribution of electrons[1-5]. Due to this reason, the possibility of a transistor that exploits negative differential capacitance has been widely studied in the recent years[6-13]. However, despite the fact that negative differential capacitance has been predicted by the standard Landau model going back to the early days of ferroelectricity[14-18], a direct measurement of this effect has never been reported, severely limiting the understanding and potential application of this effect for electronics. In this work, we demonstrate the negative differential capacitance in a thin, single crystalline ferroelectric film, by constructing a simple R-C network and monitoring the voltage dynamics across the ferroelectric capacitor.

We start by noting that capacitance is, by definition, a small signal concept-capacitance C at a given charge Q_F is related to the potential energy U by the relation $C=[d^2U/dQ_F^2]^{-1}$. Due to this reason we shall henceforth use the term 'negative capacitance' to refer to 'negative differential capacitance'. For a ferroelectric material, as shown in Fig. 1(a), the capacitance is negative only in the barrier region around $Q_F=0$. Starting from an initial state P, as a voltage is applied across the ferroelectric capacitor, the energy landscape is tilted and the polarization will move to the nearest local minimum. Fig. 1(b) shows this transition for a voltage which is smaller than the

coercive voltage V_c. If the voltage is larger than V_c, one of the minima disappears and Q_F moves to the remaining minimum of the energy landscape (Fig. 1(c)). Notably as the polarization rolls downhill in Fig. 1(c), it passes through the region where $C=[d^2U/dQ_F^2]^{-1}$ <0. Therefore, while switching from one stable polarization to other, a ferroelectric material crosses through a region where the differential capacitance is negative.

To experimentally demonstrate the above, we applied voltage pulses across a series combination of a ferroelectric capacitor and a resistor R and observed the time dynamics of the ferroelectric polarization. A 60 nm film of ferroelectric $Pb(Zr_{0.2}Ti_{0.8})O_3$ (PZT) was grown on metallic $SrRuO_3$ (60 nm) buffered $SrTiO_3$ substrate using the pulsed laser deposition technique. Square gold top electrodes with a surface area A= (30 μm)^2 were patterned on top of the PZT films using standard micro-fabrication techniques. The remnant polarization of the PZT film is measured to be ~0.74 C/m^2 and the coercive voltages are +2 V and -1.8 V. R = 50 kΩ is used as the series resistor. Fig. 2(a) shows the schematic diagram of the experimental setup and Fig. 2(b) shows the equivalent circuit diagram. The capacitor C connected in parallel with the ferroelectric capacitor in Fig. 2(b) represents the parasitic capacitance contributed by the probe-station and the oscilloscope in the experimental setup, which was measured to be ~60 pF. An AC voltage pulse V_S: -5.4 V→ +5.4 V → -5.4 V was applied as input. The total charge in the ferroelectric and the parasitic capacitor at a given time t, $Q(t)$, is calculated using $Q(t) = \int_0^t i_R(t)dt$, i_R being the current flowing through R. The charge across the ferroelectric capacitor $Q_F(t)$ is calculated using the relation: $Q_F(t) = Q(t) - CV_F(t)$, V_F being the voltage measured across the ferroelectric capacitor. Fig. 2(c) shows the transients corresponding to V_S, V_F , i_R and Q. We note in Fig. 2(c) that after the -5.4 V→ +5.4 V transition of V_S, V_F increases until point A, after which it decreases

till point *B*. We also note in Fig. 2(c) that during the same time segment, *AB*, i_R is positive and *Q* increases. In other words, during the time segment, *AB*, the changes in V_F and *Q* have opposite signs. As such, dQ/dV_F is negative during *AB* which points to the fact that the ferroelectric polarization is passing through the unstable negative states. A similar signature of negative capacitance is observed after the +5.4 V → -5.4 V transition of V_S during the time segment *CD* in Fig. 2(c). The charge density of the ferroelectric capacitor or the ferroelectric polarization, $P(t)=Q_F(t)/A$ is plotted as a function of $V_F(t)$ in Fig. 3(a). We observe in Fig. 3(a) that the $P(t)$-$V_F(t)$ curve is hysteretic and in the sections *AB* and *CD*, the slope of the curve is negative indicating that the capacitance is negative in these regions.

We also experimented with AC voltage pulses of different amplitudes and two different values of the series resistance. The $P(t)$-$V_F(t)$ characteristic is found to be qualitatively similar (see the supplementary section 2 for detailed measurements). There are, however, some interesting differences. For example, Fig. 3(b) compares the $P(t)$-$V_F(t)$ curves corresponding to R=50 kΩ and 300 kΩ for V_S: -5.4 V→ +5.4 V → -5.4 V. We note that for a smaller value of *R*, the hysteresis loop is wider, which we will explain later.

We have simulated the experimental circuit shown in Fig. 2(b) starting from the Landau-Khalatnikov equation[14],

$$\rho \frac{dQ_F}{dt} = -\frac{dU}{dQ_F} \text{ ; where energy density } U = \alpha Q_F^2 + \beta Q_F^4 + \gamma Q_F^6 - Q_F V_F. \quad (1)$$

α, β and γ are the anisotropy constants and ρ is a material dependent parameter that accounts for dissipative processes during the ferroelectric switching. Equation (1) leads to an expression for the voltage across the ferroelectric capacitor as:

$$V_F = \frac{Q_F}{C_F(Q_F)} + \rho \frac{dQ_F}{dt} \quad \text{where } C_F(Q_F) = (2\alpha Q_F + 4\beta Q_F^3 + 6\gamma Q_F^5)^{-1}. \qquad (2)$$

From equation (2), we note that the equivalent circuit for a ferroelectric capacitor consists of an internal resistor ρ and a non-linear capacitor $C_F(Q_F)$ connected in series. We shall denote $Q_F/C_F(Q_F)$ as the internal ferroelectric node voltage V_{int}. Fig. 4(a) shows the corresponding equivalent circuit. The transients in the circuit are simulated by solving equation (2) and Kirchoff's circuit equations for the circuit shown in Fig. 4(a). Fig. 4(b) shows the transients corresponding to V_S, V_F, V_{int}, i_R and Q upon the application of a voltage pulse V_S: -14 V → +14 V → -14 V with R=50 kΩ and ρ=50 kΩ. In Fig. 4(b), we observe opposite signs of changes in V_F and Q during the time segments AB and CD, as was seen experimentally in Fig. 2(b). We also note that the P-V_F curve shown in Fig. 4(c) is hysteretic as was observed experimentally in Fig. 2(d). In order to understand the difference between the P-V_F and the P-V_{int} curves that we note that $V_F=V_{int}+i_F\rho$, i_F being the current through the ferroelectric branch and the additional resistive voltage drop, $i_F\rho$ results in the hysteresis in the P-V_F curve. Nonetheless, it is clear from Fig. 4(c) that the negative slope of the P-V_{int} curve in a certain range of P due to C_F being negative in that range is reflected as the negative slope in the P-V_F curve in the segments AB and CD.

We also simulated the transients for the same circuit with R = 200 kΩ for V_S: -14 V→ +14 V→ -14 V. Fig. 4(d) compares the simulated P-V_F curves for R = 50 kΩ and 200 kΩ. We observe that, for a smaller value of R, the hysteresis loop of the simulated P-V_F curve is wider, as was observed experimentally in Fig. 3(b). This is due to the fact that for a larger R, the current through the ferroelectric is smaller resulting in a smaller voltage drop across ρ. The value of the internal resistance ρ can be extracting by comparing experimentally measured P-V_F curves for two different R for the same voltage pulse. ρ at a given P can be calculated using $\rho(P)=(V_{F1}(P)$-

$V_{F2}(P))/(i_{F1}(P)-i_{F2}(P))$ where $V_{F1}(P)$ and $V_{F2}(P)$ are the ferroelectric voltages at a given P for two R and $i_{F1}(P)$ and $i_{F2}(P)$ are the corresponding current through the ferroelectric at the same P. The average ρ found to decrease monotonically with an increasing amplitude of the applied voltage, while the average value of the negative capacitance remains reasonably constant (see supplementary Fig. S17).

If the applied voltage amplitude is smaller than coercive voltage so that the ferroelectric resides in one of the potential wells (see Fig 1a), its capacitance is positive and so it should behave just as a simple capacitor. On the other hand, if the applied voltage amplitude is larger than the coercive voltage, the ferroelectric switches and a negative capacitance transient is expected. This is exactly what is observed in our experiments (see Supplementary section 4.3). The fact that in the same circuit both positive and negative capacitance transients can be achieved just by changing the amplitude of the voltage also indicate that any influence of the parasitic components, if present, are minimal. In addition, detailed measurements (see Supplementary section 3) show that influence of defects is also minimal. Furthermore, the observed effect is robust against material variations. Supplementary section 8 shows data for a different material stack where PZT thickness is increased to 100 nm and bottom electrode is changed to $La_{0.5}Sr_{0.5}MnO_3$ (20 nm) from SRO. A similar negative capacitance transient is observed.

The addition of a series resistance (R) is critically important to reveal the negative capacitance region in the dynamics. An appreciable voltage drop across the series R makes sure that the voltage across the ferroelectric capacitor can be measured without being completely dominated by the source voltage–at the limit when $R \rightarrow 0$, the voltmeter would be directly connected across

the voltage source. Indeed, most model studies[15,19-21] have been done in the latter limit where the ferroelectric capacitor is directly connected across a voltage source (or through a small resistance). Note that the dynamics in our experiments are intentionally slowed down by adding a large series resistance. The duration of the negative capacitance transient can be probed by varying the value of the series resistance and is found to be approximately 20 ns (see Supplementary section 8).

A negative slope in the polarization-voltage characteristic has been predicted since the early days of ferroelectricity[14-18]. A S-like polarization voltage behavior in one branch of the hysteresis was measured in a transistor structure in Ref. 11. However, a successful measurement of the entire intrinsic hysteresis loop has been performed only indirectly[18]. By contrast, our results provide a direct measure of the intrinsic hysteresis and negative capacitance of the material. Given the size of the capacitor used (30 μm x 30 μm), the switching invariably happens through domain-mediated mechanisms. Importantly, our results show that, even in such a domain mediated switching, a regime of abrupt switching is present that leads to negative capacitance transience. Thus, the double well picture shown in Fig. 1(a) which is typically associated with a single domain configuration (Eq. 1), can still qualitatively predict the experimental outcome. Interestingly, from Fig. 2(c), it is clear that the negative capacitance ensues in the initial period of the switching. This indicates that microscopically abrupt switching events dominate the early part of the dynamics, thereby providing a unique insight into the switching process. By varying external stimuli, it is also possible to probe the behavior of intrinsic parameters such as ρ (see Supplementary Information Section 6) that govern the ferroelectric switching. Before concluding, it is worth noting that the concept of negative capacitance goes beyond the

ferroelectric hysteresis and can be applied in general to a two state system separated by an intrinsic barrier (stored energy)[22-26]. The measurement presented here could provide a generic way to probe the intrinsic negative capacitance in all such systems. A robust measurement of the negative capacitance could provide a guideline for stabilization which could then overcome Boltzmann Tyranny in field effect transistors, as mentioned earlier. The inductance-like behavior observed in this experiment could also lead to many other applications such as to negate capacitances in an antenna, to boost up voltages at various part of a circuit, to develop coil-free resonators and oscillators, etc.

Acknowledgements: This work was supported in part by FCRP Center for Materials, Structures and Devices (MSD), the STARNET LEAST center, the NSF E3S center at Berkeley and Office of Naval Research (ONR). A.I.K. acknowledges the Qualcomm Innovation Fellowship 2012-13.

References

1. Salahuddin, S., Datta & S. Use of negative capacitance to provide voltage amplification for low power nanoscale devices. *Nano Lett*. **8**, 405-410 (2008).

2. Zhirnov, V. V. & Cavin, R. K. Negative capacitance to the rescue. *Nature Nanotechnology* **3**, 77-78 (2008).

3. Theis, T. N. & Solomon, P. M. It's time to reinvent the transistor! *Science* **327**, 1600-1601 (2010).

4. Theis, T. N. & Solomon, P. M. In quest of the next switch: prospects for greatly reduced power dissipation in a successor to the silicon field-effect transistor. *Proc. IEEE* **98**, 2005-2014 (2010).

5. Ionescu, A. M. & Riel, H. Tunnel field-effect transistors as energy-efficient electronic switches, *Nature* **479**, 329-337 (2011).

6. C. Dubourdieu *et al*. Switching of ferroelectric polarization in epitaxial $BaTiO_3$ films on silicon without a conducting bottom electrode. *Nature Nanotech.* **8**, 748-754 (2013).

7. Salahuddin, S. & S. Datta, S. Proc. *Intl. Electron Devices Meeting (IEDM),* 2008.

8. Rusu, A., Salvatore, G. A., Jiménez, D., Ionescu, A. M. Metal-Ferroelectric-Metal-Oxide-Semiconductor Field Effect Transistor with Sub-60mV/decade Subthreshold Swing and Internal Voltage Amplification. *Proc. Intl. Electron Devices Meeting (IEDM),* 2010.

9. Khan A. I. *et al*. Experimental evidence of ferroelectric negative capacitance in nanoscale heterostructures *Appl. Phys. Lett*. **99**, 113501-3 (2011).

10. Khan A. I. *et. al*. Ferroelectric negative capacitance MOSFET: capacitance tuning & antiferroelectric operation *Proc. Intl. Electron Devices Meeting (IEDM),* 2011.

11. Salvatore, G. A., Rusu, A. & Ionescu, A. M. Experimental confirmation of temperature dependent negative capacitance in ferroelectric field effect transistor. *Appl. Phys. Lett*. 100, 163504-1-3 (2012).

12. Then, H. W. *et al*. Experimental observation and physics of "negative" capacitance and steeper than 40mV/decade subthreshold swing in $Al_{0.83}In_{0.17}N$/AlN/GaN MOS-HEMT on SiC substrate. *Proc. Intl. Electron Devices Meeting (IEDM)*, 2013.

13. The International Technology Roadmap for Semiconductors, Emerging Research Devices (http://www.itrs.net/Links/2011itrs/home2011.htm, (2011).

14. Landau, L. D. & Khalatnikov, I. M. On the anomalous absorption of sound near a second order phase transition point. *Dok. Akad. Nauk* **96**, 469-472 (1954).

15. Lines, M. E. & Glass, A. M. Oxford University press, 1977.

16. Merz, W. J. Switching time in ferroelectric BaTiO3 and its dependence on crystal thickness. *J. of Appl. Phys*. **27**, 938-943 (1956).

17. Bratkovsky, A. M. & Levanyuk, A. P. Very large dielectric response of thin ferroelectric films with the dead layers. *Phys. Rev. B* **63**, 132103-1-3 (2001).

18. Bratkovsky, A. M. & Levanyuk, A. P. Depolarizing field and "real" hysteresis loops in nanometer-scale ferroelectric films. *Appl. Phys. Lett*. 89, 253108-1-3 (2006).

19. Larsen, P. K. *et al.* Nanosecond switching of thin ferroelectric films. *Appl. Phys. Lett*. **59,** 611-613 (1991).

20. Li, J. *et al.* Ultrafast polarization switching in thin-film ferroelectrics. *Appl. Phys. Lett*. **84,** 1174-1176 (2004).

21. Jiang, A. Q. et al. Subpicosecond domain switching in discrete regions of $Pb(Zr_{0.35}Ti_{0.65})O_3$ thick films. *Adv. Func. Mat.* **22**, 2148-2153 (2012).

22. Jana, R. K., Snider, G. L. and Jena, D. On the possibility of sub 60 mV/decade subthreshold switching in piezoelectric gate barrier transistors. *Physica Status Solidi (c)* 10, 1469-1472 (2013).

23. AbdelGhany, M. and Szkopek, T. Extreme sub-threshold swing in tunnelling relays. *Appl. Phys. Lett*. **104**, 013509 (2014).

24. Masuduzzaman, M., and Alam, M. A. "Effective Nanometer Airgap of NEMS Devices using Negative Capacitance of Ferroelectric Materials." *Nano Lett. 14*, 3160–3165 (2014).

25. Eisenstein, J. P., L. N. Pfeiffer, and K. W. West. "Negative compressibility of interacting two-dimensional electron and quasiparticle gases." *Phys. Rev. Lett.* 68, 674-677 (1992).

26. Li, Lu, et al. "Very large capacitance enhancement in a two-dimensional electron system." *Science* 332, 825-828 (2011).

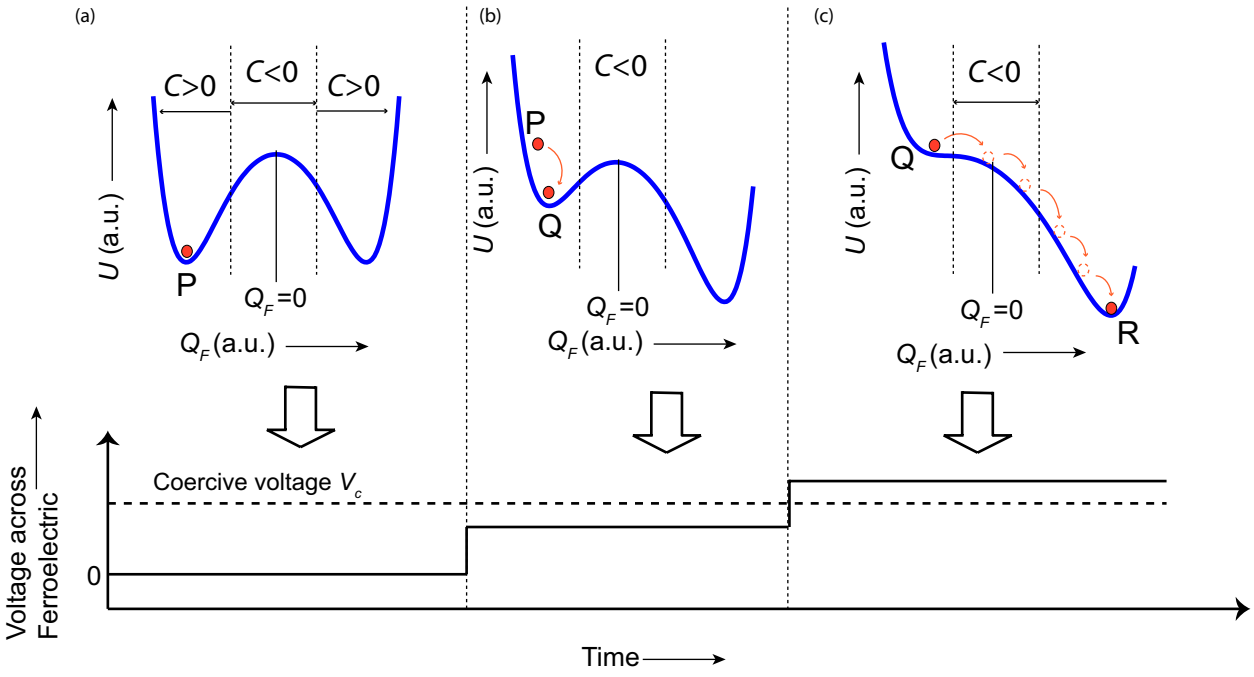

Figure 1: **Energy Landscape description of the ferroelectric negative capacitance.** (a) The energy landscape of a ferroelectric capacitor in the absence of an applied voltage. The capacitance is negative only in the barrier region around $Q_F=0$. (b,c) The evolution of the energy landscape upon the application of a voltage across the ferroelectric capacitor that is smaller (b) and larger than the coercive voltage (c). If the voltage is larger than the coercive voltage, the ferroelectric polarization rolls down hill through the negative capacitance states.

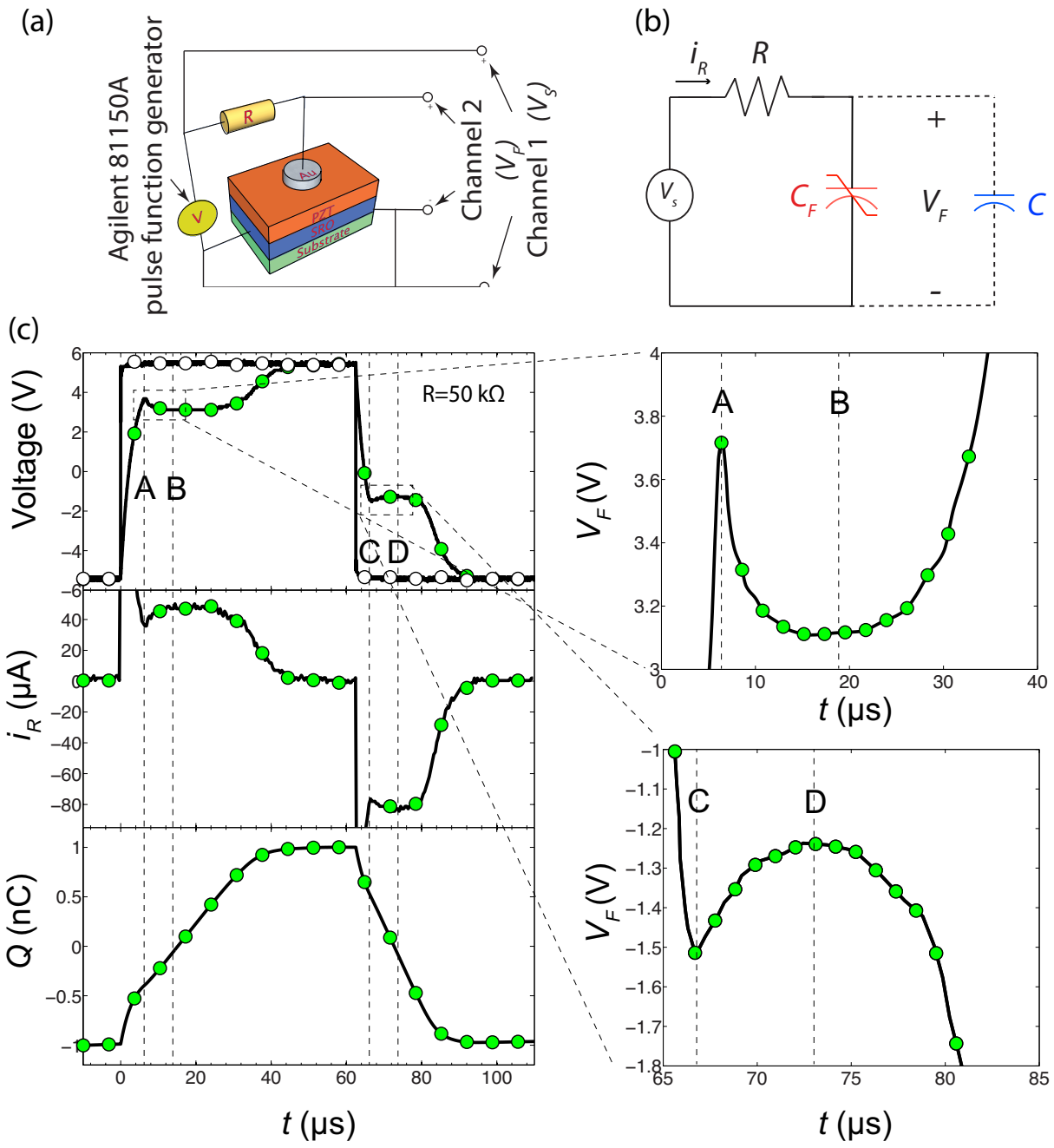

Figure 2: **Transient response of a Ferroelectric Capacitor.** (a) Schematic diagram of the experimental setup. (b) Equivalent circuit diagram of the experimental setup. (c) Transients corresponding to the source voltage V_S, the ferroelectric voltage V_F and the charge Q upon the application of a AC voltage pulse V_S: -5.4 V→ +5.4 V → -5.4 V. R=50 kΩ.

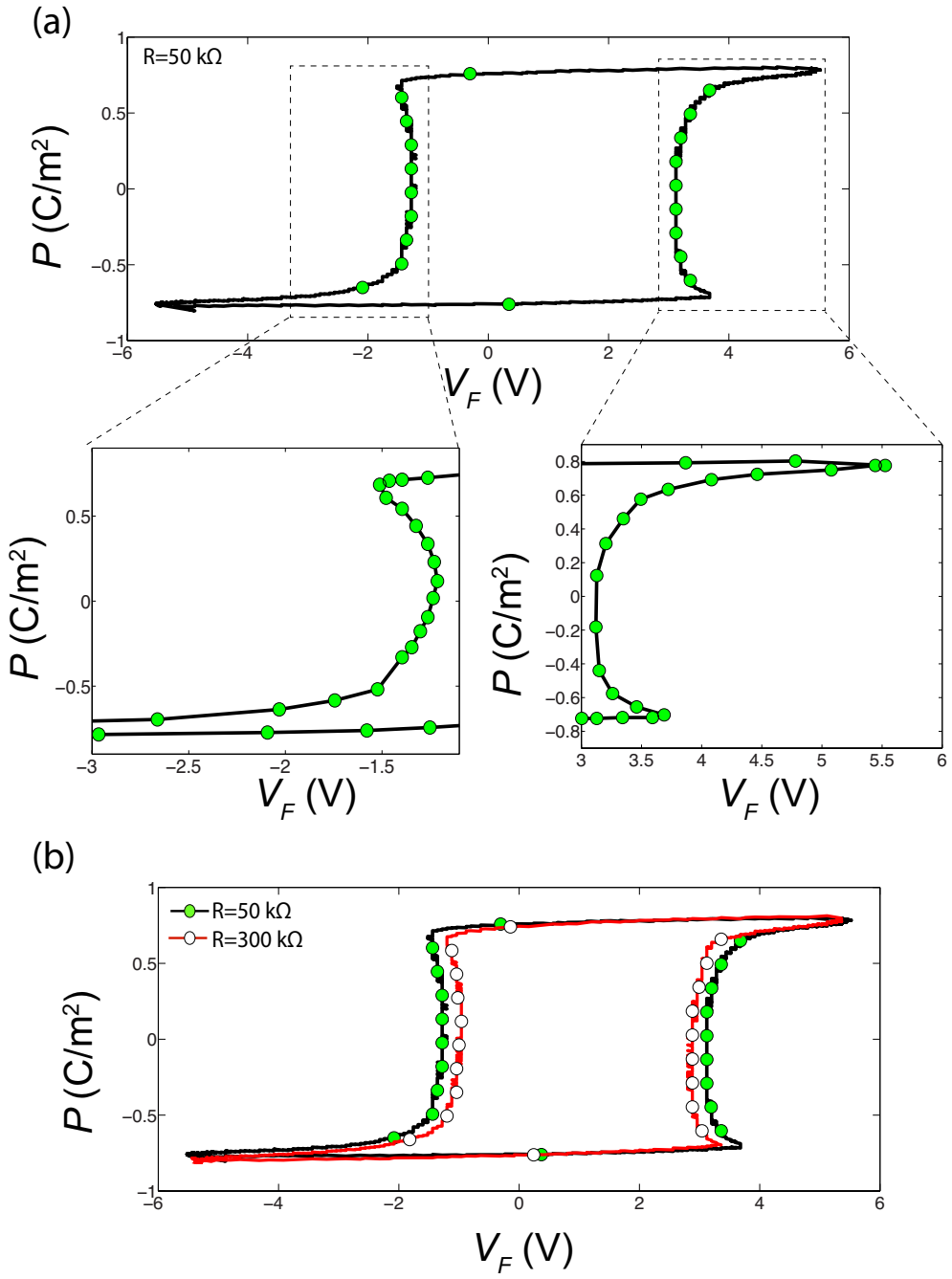

Figure 3: **Experimental measurement of Negative Capacitance.** (a) The ferroelectric polarization *P(t)* as a function of $V_F(t)$ with *R*=50 kΩ for V_S: -5.4 V→ +5.4 V → -5.4 V. (b) Comparison of the *P(t)*-$V_F(t)$ curves corresponding to *R*=50 kΩ and 300 kΩ for V_S: -5.4 V→ +5.4 V → -5.4 V.

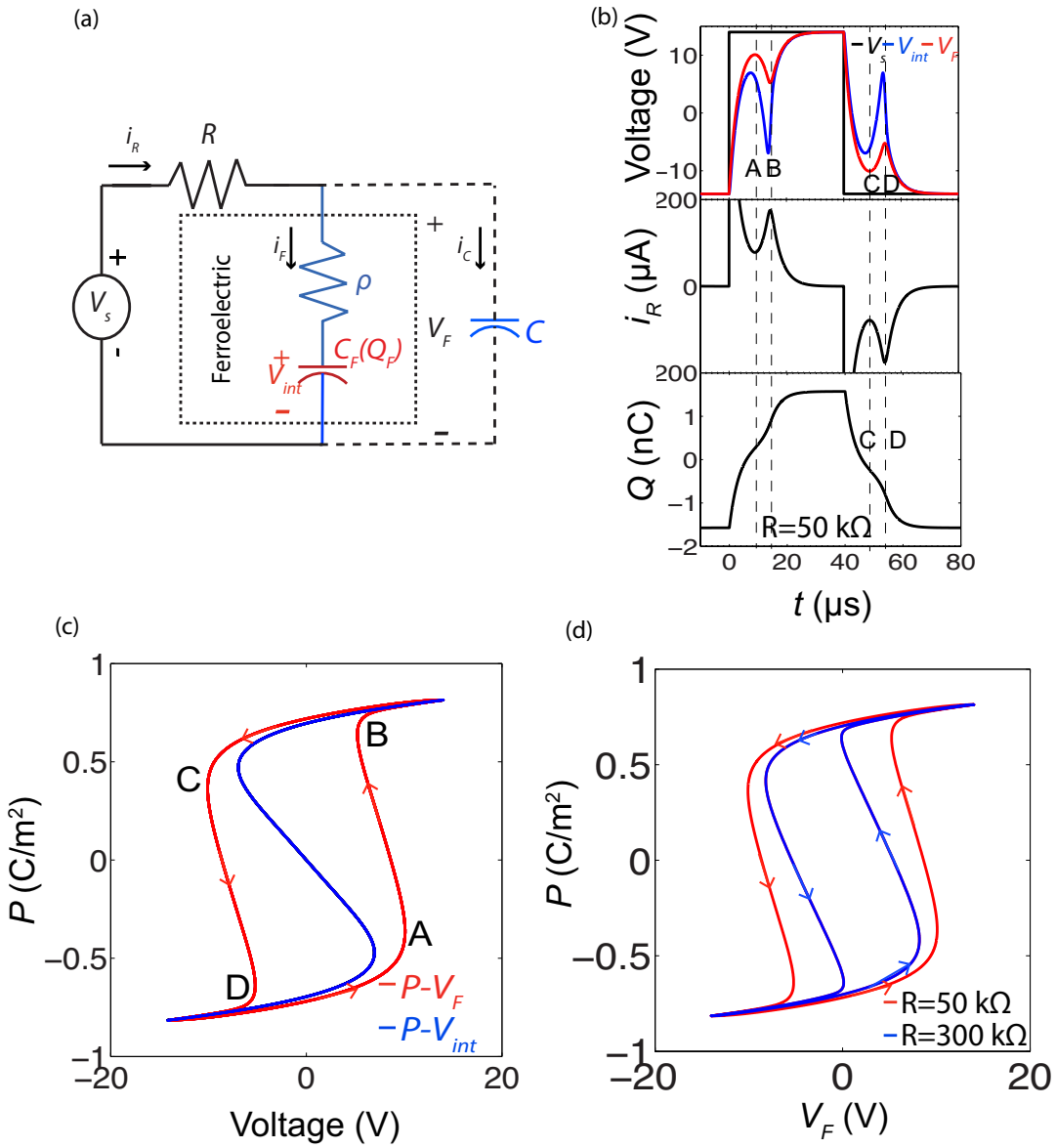

Figure 4: **Simulation of the time-dynamics of the ferroelectric switching.** (a) Equivalent circuit diagram of the simulation. (b) Simulated transients corresponding to the source voltage V_S, the ferroelectric voltage V_F and the charge Q upon the application of a voltage pulse V_S: -14 V→ +14 V → -14 V. (c) The ferroelectric polarization $P(t)$ as a function of $V_F(t)$ and $V_{int}(t)$. (d) Comparison of the simulated $P(t)$- $V_F(t)$ curves for R = 50 kΩ and 200 kΩ upon the application of V_S: -14 V → +14 V → -14 V.

Supplementary Online Information: Negative Capacitance in a Ferroelectric Capacitor

Asif Islam Khan,[1] Korok Chatterjee,[1] Brian Wang,[1] Steven Drapcho,[2] Long You,[1], Claudy Serrao,[1], Saidur Rahman Bakaul,[1], Ramamoorthy Ramesh,[2,3,4] Sayeef Salahuddin[1,4*]

[1]Dept. of Electrical Engineering and Computer Sciences, University of California,
[2]Dept. of Physics, University of California,
[3]Dept. of Material Science and Engineering, University of California,
[4]Material Science Division, Lawrence Berkeley National Laboratory Berkeley, CA 94720

*To whom correspondence should be addressed; E-mail: sayeef@berkeley.EDU

1 Growth and structural characterization

A 60 nm $Pb(Zr_{0.2}Ti_{0.8})O_3$ (PZT) thin film was grown on a 60 nm metallic $SrRuO_3$ (SRO) buffered $SrTiO_3$ (STO) substrate using the pulsed laser deposition technique. PZT, SRO and STO are closely lattice matched, for which the epitaxial growth of the heterostructure results in a high crystalline quality and a robust ferroelectricity in PZT and minimizes defects. SRO and PZT films were grown at 630 ^{0}C and 720 ^{0}C respectively. During the growth, the oxygen partial pressure was kept at 100 mTorr and afterwards the heterostructure was slowly cooled down at 1 atm of oxygen partial pressure and a rate of -5 ^{0}C/min to the room temperature. Laser pulses of 100 mJ of energy and $\sim$4mm^2 of spot size were used to ablate the targets. Gold top electrodes were ex-situ deposited by e-beam evaporation and then patterned using standard lithographic techniques into square dots of a surface area, A= (30 μm)^2. The SRO layer was used as the bot-

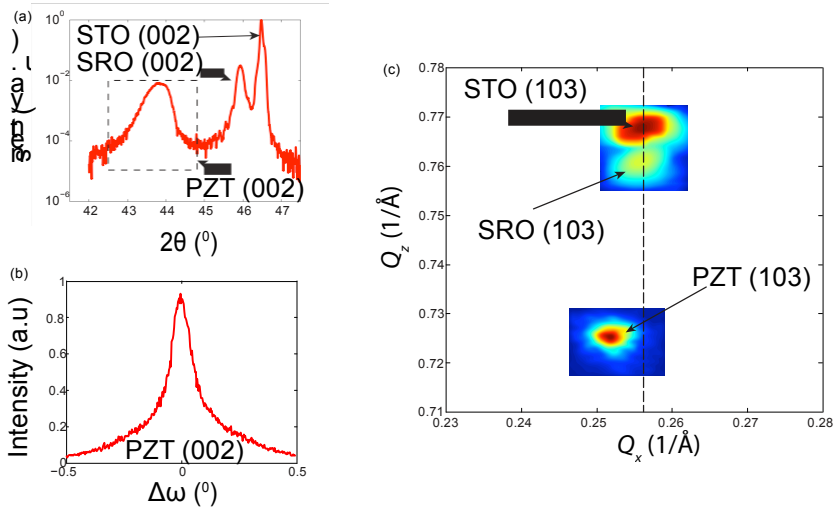

Figure S1: (a) The X-ray diffraction spectrum of the PZT(60 nm)/SRO(60nm) heterostructure on the STO substrate around the (002) reflections. (b) The rocking curve measurement around the PZT (002) reflection. (c) The reciprocal space map of the heterostructure around the (103) reflections of the heterostructure.

tom electrode. The chosen thicknesses of PZT and SRO ensure a very low leakage and a good bottom contact. Fig. S1(a) shows the X-ray diffraction spectrum of the heterostructure around the (002) reflections. Fig. S1(b) shows the rocking curve measurement around the PZT (002) reflection. The full-width-at-the-half-maximum of the PZT (002) peak, $\Delta\omega$, is $\sim 0.1^0$. Fig. S1(c) shows the reciprocal space map of the heterostructure around the (103) reflections. We note that the PZT (103) peak has a smaller Q_x than that of the substrate (103) peak indicating that the PZT film is partially/fully strain relaxed.

2 Measurement of the remnant polarization

The ferroelectric hysteresis loop is traditionally measured using the Sawyer-Tower technique (*1*). Fig. S2(a) shows the ferroelectric hysteresis loop of the 60 nm PZT film grown on SRO buffered STO (001) substrate measured by this technique using a Radiant Precision Multiferroic tester. To supplement the Sawyer-Tower measurement of the remnant polarization, we also

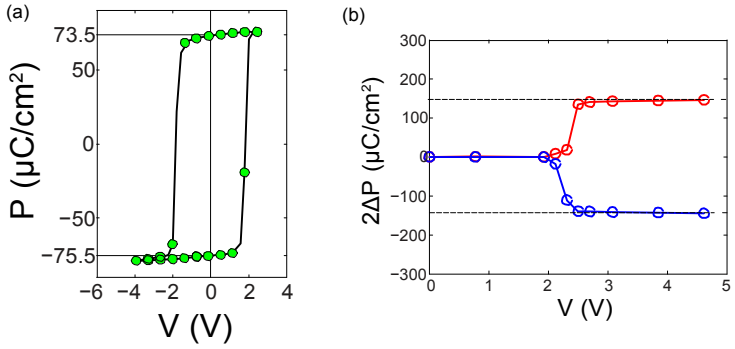

Figure S2: (a) The polarization (P)-voltage (V) hysteresis curve of the ferroelectric measured using a Sawyer-Tower type setup. (b) The positive-up-negative-down (PUND) measurement of the PZT capacitor.

measured the switched polarization using the positive-up-negative-down (PUND) technique, which is usually used to distinguish between ferroelectric switching and artifacts caused by defects (*2*). Fig. S2(b) shows the positive-up-negative-down (PUND) measurement of the PZT capacitor. The remnant polarization as measured using both of the techniques are the same ($\sim$0.74 C/m^2) indicating that defects play a minimal role in determining the properties of our sample.

3 Dielectric characterization and frequency dispersion

Fig. S3(a, b, c, d) show the dielectric constant-voltage and the admittance angle-voltage characteristics of the PZT sample at 1 kHz, 10 kHz, 100 kHz and 1 MHz respectively and fig. S3(e) shows the frequency dispersion of the dielectric constant between 1 kHz and 1 MHz. In fig. S3(a-e), we observe that the admittance angle is $\sim 90^0$ at all frequencies. This points to negligible DC leakage through our samples. We further note in fig. S3(e) that the dispersion of the dielectric constant over 3 orders of magnitude variation in frequency is less than 5%. Generally, the defect dynamics that include trapping of electrons and charging/discharging of the same in the defect states result in large frequency dispersion of the dielectric constant in

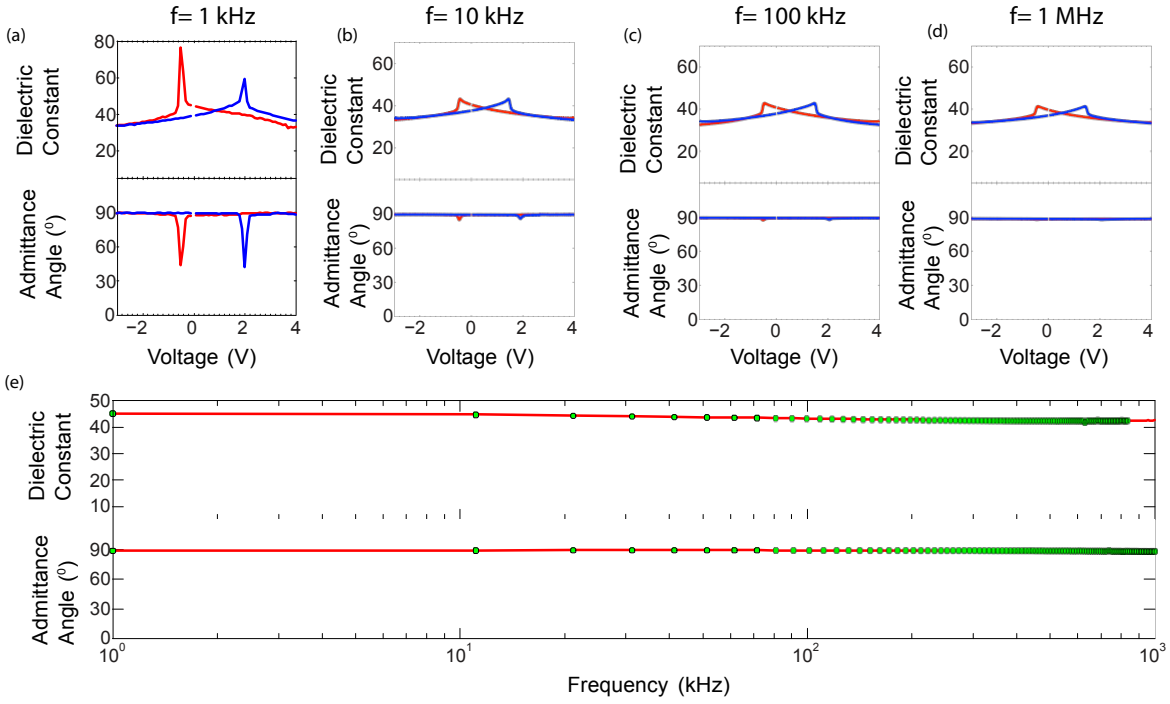

Figure S3: (a,b,c,d) Dielectric constant-voltage and the admittance angle-voltage characteristics of the PZT sample at 1 kHz (a), 10 kHz (b), 100 kHz (c) and 1 MHz (d) . (e) The frequency dispersion of the dielectric constant between 1 kHz and 1 MHz

ferroelectrics (*3*). This points to the fact there is a negligible amount of defects in the PZT sample.

Another technique that is widely used to characterize the defects in ferroelectrics is the Rayleigh analysis (*3–5*). The basis of this analysis is that, due to the movement of the defects in response to an AC electric field E_0, the dielectric constant of a ferroelectric increases as E_0 increases even when E_0 is smaller the coercive field. Fig. S4 shows the dielectric constant ε_r as a function the AC electric field E_0 at 10 kHz. We observe that as the AC electric field is increased from 10 kV/cm to the coercive field (~250 kV/cm), the dielectric constant increases by a mere 1.5%. This independently shows that the defects are minimal for our PZT sample.

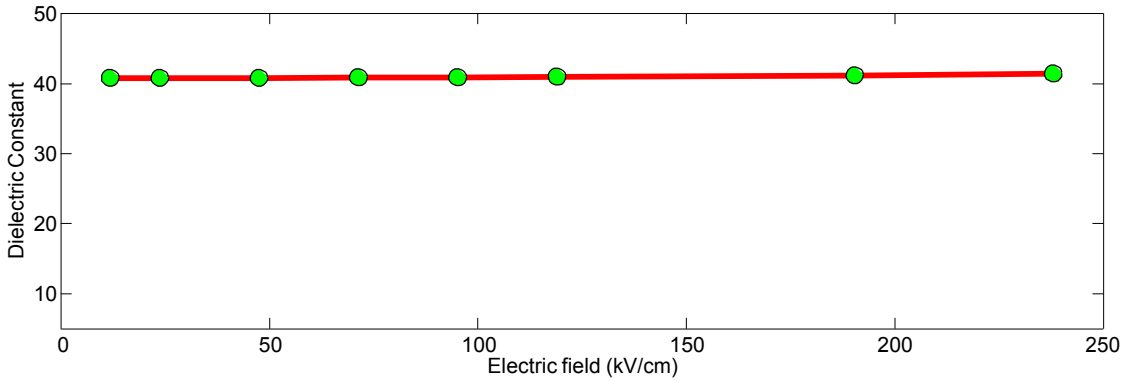

Figure S4: The dielectric constant ε_r as a function the AC electric field E_0 at 10 kHz.

4 Transient response of the ferroelectric capacitor

4.1 Experimental setup for measuring the transient response

The PZT capacitor was connected to a voltage pulse source (Agilent 81150A pulse function generator) through an external series resistor R. The voltage transients were measured using a digital storage oscilloscope (Tektronix 2024). Top Au and bottom SRO contacts were connected to the probe tips in a probe station through which the ferroelectric capacitor was connected to the other circuit components. Main text fig. 2(a) shows the experimental setup and the electrical connections to the oscilloscope.

4.2 Extraction of the parasitic capacitance

In order to extract the value of the parasitic capacitance which is referred to as C in main text fig. 2(b), voltage pulses were applied across the probe station under open circuit conditions through the resistor R = 50 kΩ. Fig. S5(a) shows the transient response of the circuit for an applied voltage V_s : -5.4 V→+5.4 V. By fitting the voltage transient across the probes V_x shown in Fig. S5(a) to the equation $V_x(t) = (+5.4 - 2 \times 5.4e^{-t/(RC)})$ V with R = 50 kΩ, the value of the parasitic capacitance C is extracted to be ~60 pF. Fig. S5(c) compares the transients of the

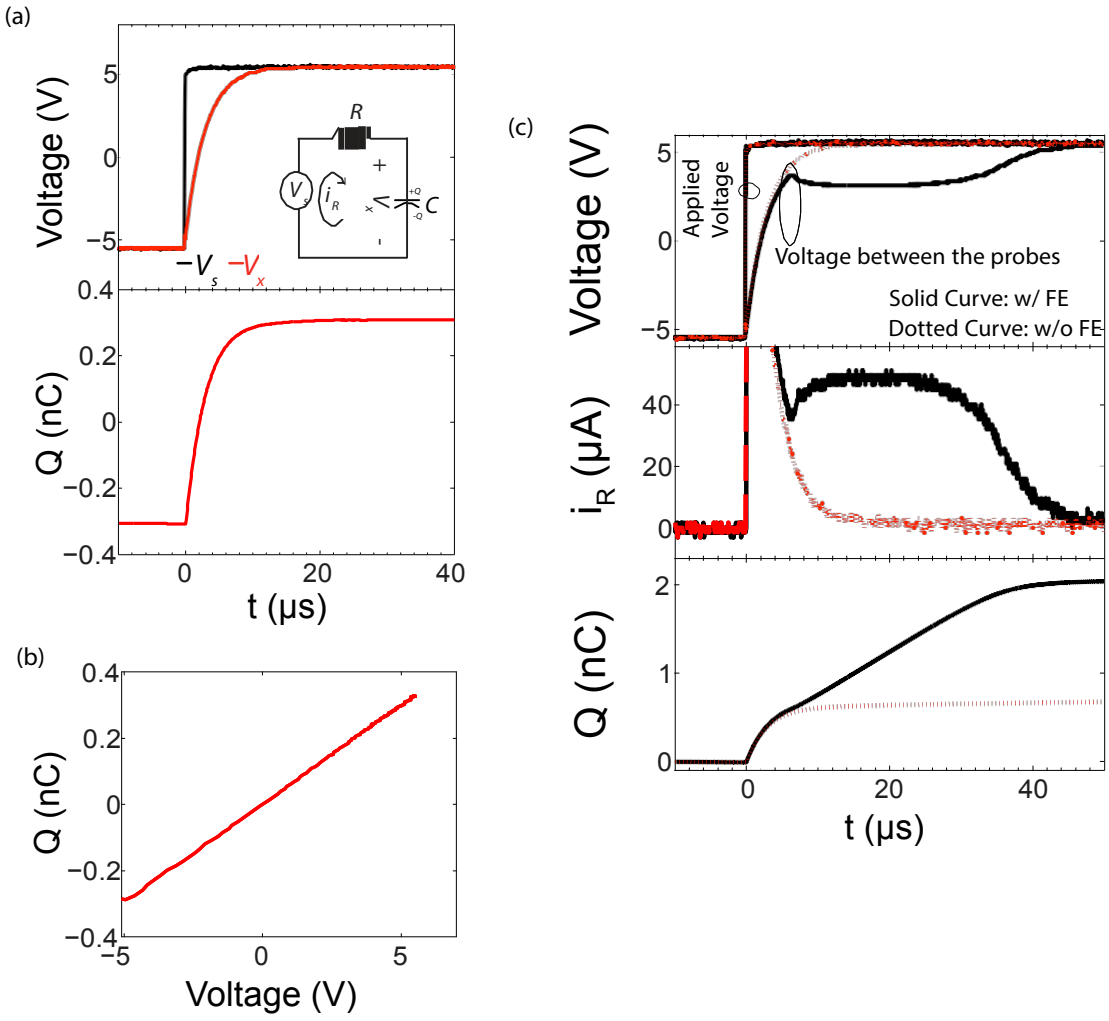

Figure S5: (a) Transient response of the circuit under the open circuit conditions to an AC voltage pulse V_s : -5.4 V →+5.4 V. (b) The charge-voltage characteristics of the parasitic capacitor. (c) Comparison of the transients for the circuit under an open circuit condition with those in the closed circuit with the ferroelectric capacitor between the probes for an AC voltage pulse V_s : -5.4 V →+5.4 V.

open circuit with those of the closed circuit with the ferroelectric capacitor connected between the probes in response an AC voltage pulse V_s : -5.4 V→+5.4 V. In Fig. S5(c), we observe that, after the transition of V_s, the transients are initially dominated by the parallel capacitor, which is corroborated by simulations.

4.3 Correlation between the ferroelectric switching and the negative capacitance transient

To correlate the characteristic negative capacitance transients with the ferroelectric switching, we note the following.

1. When a voltage is applied which is lower than the coercive voltage so that there is no switching of the polarization, we observe simply a capacitive charging of the voltage, as expected from the double well energy landscape of the ferroelectric material. The coercive voltage of our PZT sample is ±2 V, which is evident from the hysteresis loop plotted in Fig. S2(a). In Fig. S6(a,b), the voltage transients are shown for voltages pulses V_s: -1 V→ +1 V → -1 V and V_s: -1.8 V→ +1.8 V → -1.8 V respectively. Clearly, there are no negative capacitance transients observed in Fig. S6, since the applied AC voltage amplitude is less the coercive voltage.

2. Now, in the same setup, when a voltage is applied which is larger than the coercive voltage so that the ferroelectric polarization switches its direction, we observe the negative capacitance transient. In Fig. S7, the AC voltage magnitude is larger than the coercive voltage and the negative capacitance transients are observed.

3. To further elucidate the point, we applied successive DC pulses on the PZT sample. In Fig. S8(a), a large negative voltage pulse was first applied to align the polarization away from the PZT/SRO interface and then two successive +6 V pulses were applied. We note in Fig. S8(a) that during the 1st pulse, the switching of polarization occurs which results in the characteristic negative capacitance transient of the ferroelectric voltage V_F; on the other hand, during the 2nd pulse, the polarization does not switch since it had already been aligned with the applied electric field in the previous pulse, and no negative capacitance transient is observed in the V_F waveform during the 2nd pulse. Similar experiment with

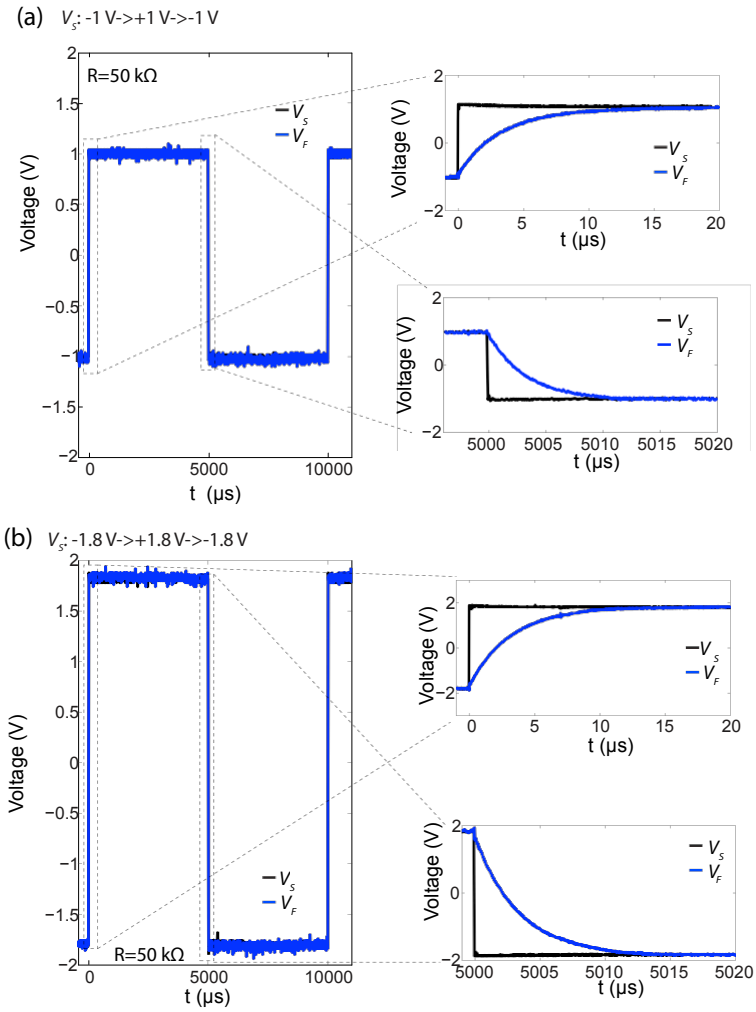

Figure S6: Transient response of the series combination of the ferroelectric capacitor and a resistor R = 50 kΩ to an AC voltage pulse V_s :-1 V→+1 V→-1 V (a) and V_s :-1.8 V→+1.8 V→-1.8 V (b).

two successive -6 V pulses is shown in Fig. S8(b).

This correlation between switching and the characteristic transients clearly shows that the characteristic negative capacitance transients are due to the intrinsic ferroelectric switching dynamics and not because of any extrinsic defect dynamics.

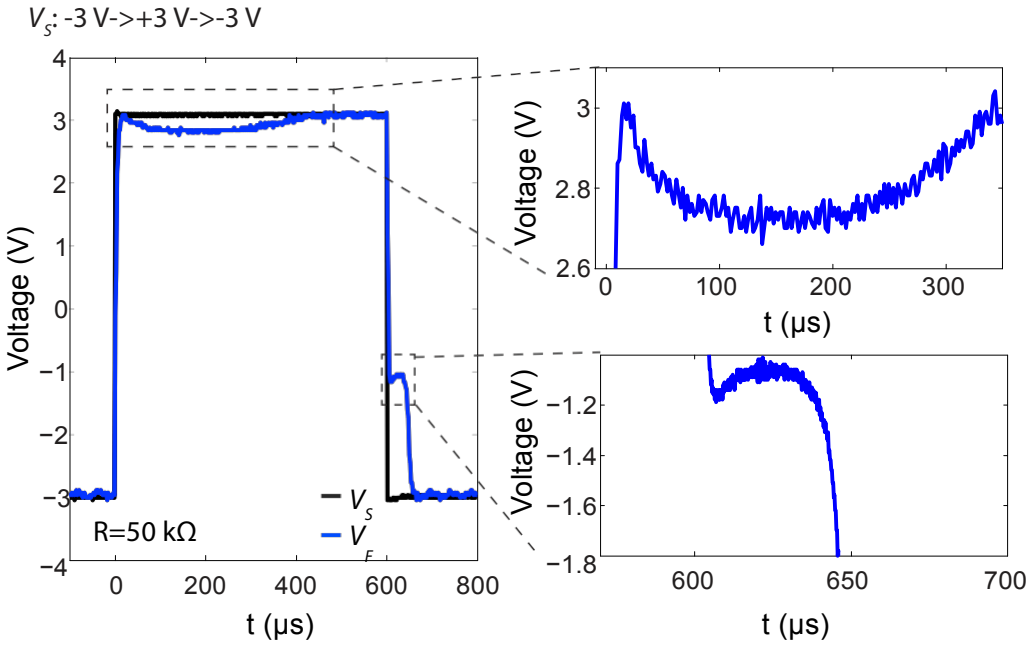

Figure S7: Transient response of the series combination of the ferroelectric capacitor and a resistor R = 50 kΩ to an AC voltage pulse V_s :-3 V→+3 V→-3 V.

4.4 P-V_F curves for different voltage amplitudes

Fig. S9(a,b,c,d,e) show the transient response of the series combination of the ferroelectric capacitor and a resistor R = 50 kΩ to AC voltage pulses with amplitudes of 3.25 V, 3.5 V, 4.2 V, 4.5 V, 5.2 V and 6 V, respectively. Fig. S10 compares the P-V_F curves of the same circuit for V_s : -3.5 V →+3.5 V → -3.5 V and V_s :-5.4 V →+5.4 V →-5.4 V. Fig. S11 compares the P-V_F curve corresponding to V_s :-3.5 V→+3.5 V→-3.5 V with that for different other AC voltage pulses. We note in Fig. S10 and S11 that for a larger peak voltage, the hysteresis window is wider. This is due to the fact that for a larger peak voltage, a larger current flows into the ferroelectric, thereby increasing the voltage drop across the internal resistance ρ.

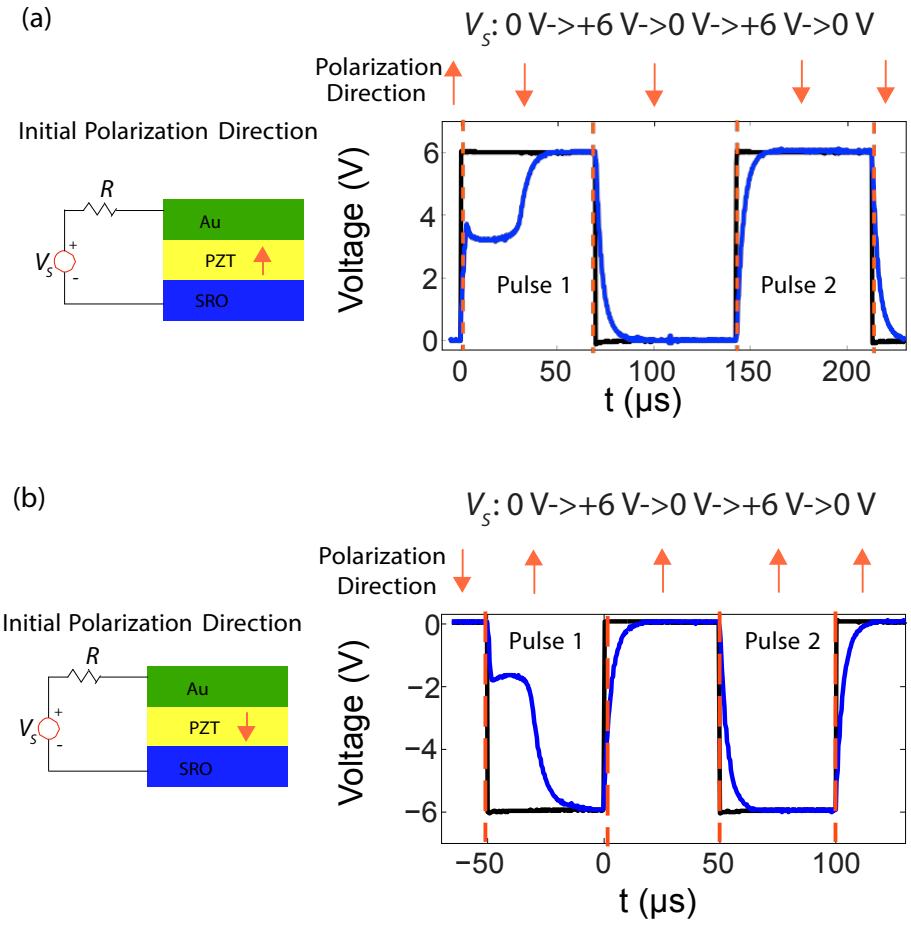

Figure S8: Transient response of the series combination of the ferroelectric capacitor and a resistor R = 50 kΩ to two successive DC voltage pulses of V_s : 0 V→ +6 V→0 V (a) and V_s : 0 V→ -6 V→0 V (b). The relative polarization directions at different time are also indicated.

4.5 P-V_F curves for different external series resistors

Fig. S12(a) shows the transient response of the series combination of the ferroelectric capacitor and a resistor R = 300 kΩ to an AC voltage pulse V_s : -5.4 V→+5.4 V→-5.4 V. Main text Fig. 3(c) compares the P-V_F curves corresponding to R=50 kΩ and 300 kΩ for V_s : -5.4 V →+5.4 V → -5.4 V.

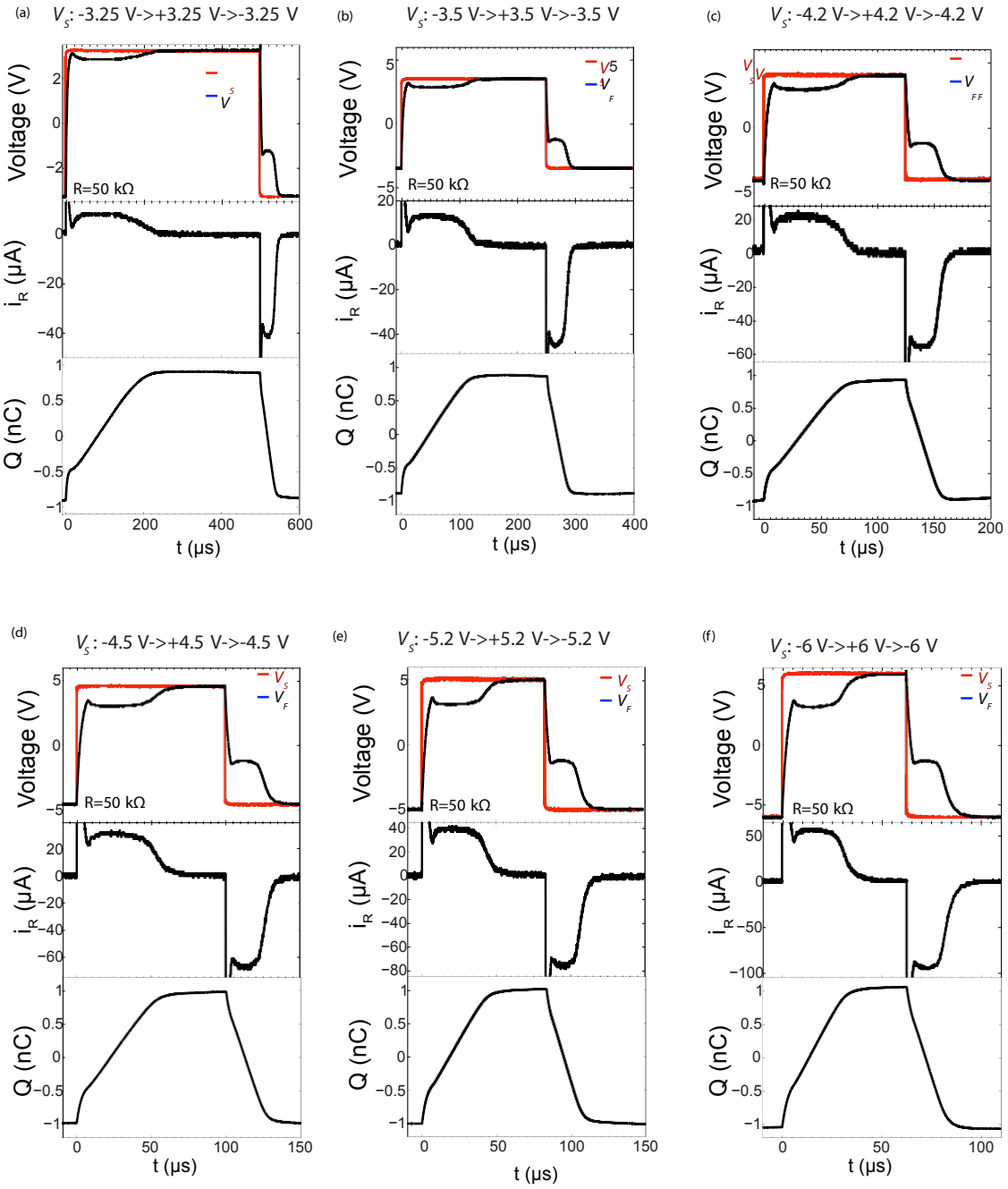

Figure S9: Comparison of the transient response of the series combination of the ferroelectric capacitor and a resistor $R = 50\ \text{k}\Omega$ to different AC voltage pulses.

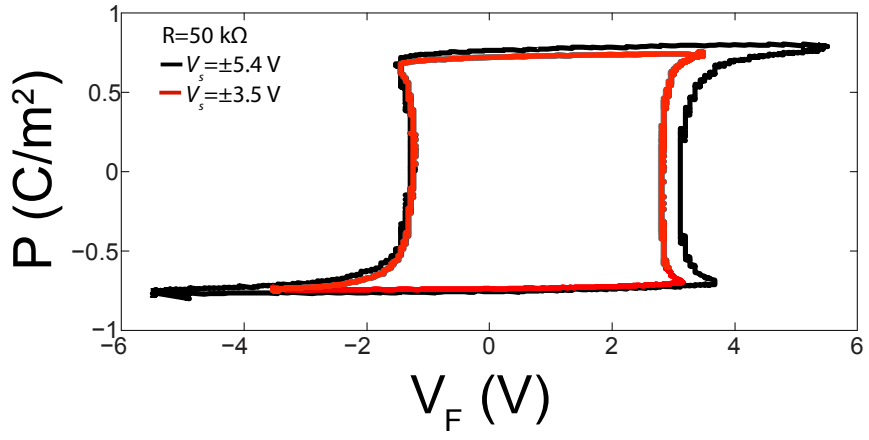

Figure S10: Comparison of the P-V_F curves for the same circuit for V_s : -3.5 V →+3.5 V→-3.5 V and V_s :-5.4 V→+5.4 V→-5.4 V.

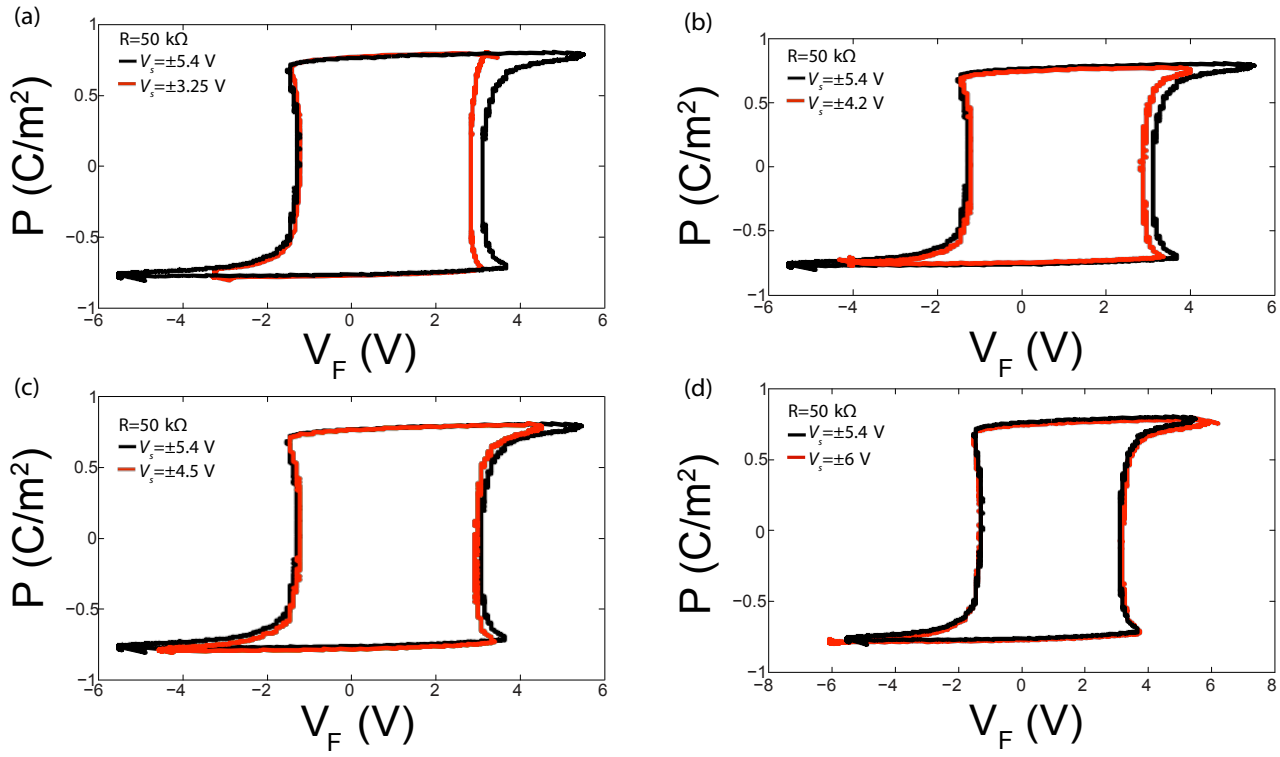

Figure S11: Comparison of the P-V_F curves corresponding to V_s :-5.4 V→+5.4 V→-5.4 V with that for different other voltage pulses.

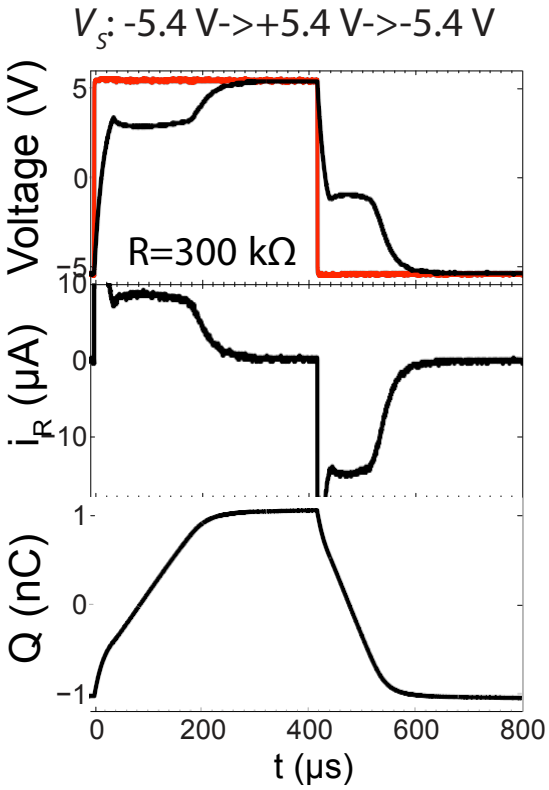

Figure S12: Transient response of the series combination of the ferroelectric capacitor and a resistor R = 300 kΩ to an AC voltage pulse V_s :-5.4 V→+5.4 V→-5.4 V.

5 Model

5.1 Anisotropy constants

For an applied electric field E across the ferroelectric capacitor, the per unit volume energy of a ferroelectric U_{pu} is given by

$$U_{pu} = \alpha_1 P^2 + \alpha_{11} P^4 + \alpha_{111} P^6 - PE \tag{1}$$

where P is the surface charge density or the ferroelectric polarization and α_1, α_{11} and α_{111} are the anisotropy constants of the material. For a parallel plate capacitor of area A and thickness d, the charge Q_F is given by $Q_F = PA$. The voltage across the ferroelectric capacitor $V_F = Ed$ and the free energy of the capacitor $U = U_{pu}Ad$. Hence the energy of the capacitor can be

written as

$$\begin{aligned} U &= U_{pu} A d \\ &= \{\alpha_1 (\frac{Q_F}{A}) + \alpha_{11} (\frac{Q_F}{A})^4 + \alpha_{111} (\frac{Q_F}{A})^6 - (\frac{Q_F}{A}) E\} A d \\ &= \frac{d\alpha_1}{A} Q_F^2 + \frac{d\alpha_{11}}{A^3} Q_F^4 + \frac{d\alpha_{111}}{A^5} Q_F^6 - Q_F V_F \end{aligned} \quad (2)$$

Comparing equation (2) with the main text equation (1), the following relationships are obtained.

$$\alpha = \frac{d\alpha_1}{A} \quad (3)$$

$$\beta = \frac{d\alpha_{11}}{A^3} \quad (4)$$

$$\gamma = \frac{d\alpha_{111}}{A^5} \quad (5)$$

The values of the anisotropy constants (α_1, α_{11} and α_{111}) are taken from Ref. (*2*).

5.2 Landau-Khalatnikov simulations

The circuit diagram for the simulation is shown in main text Fig. 4(a). A 60 nm PZT film with square electrodes of area A= (30 μm)^2 is taken as the ferroelectric capacitor. The parasitic capacitance C=60 pF. ρ is taken as 50 kΩ. The remnant polarization corresponding to these anisotropy constants is ~0.7 C/m^2 and the coercive voltage is ±7.5 V.

The circuit shown in main text Fig. 4(a) is simulated by solving the following equations at each time step.

$$0 = V_s(t) - i_R(t)R - (i_R(t) - i_C(t))\rho - V_{int}(t) \quad (6)$$

$$0 = V_{int}(t) + (i_R(t) - i_C(t))\rho - \frac{1}{C} \int_{t=0}^{t} i_C(t)dt \quad (7)$$

$$Q_F(t) = Q_F(t=0) + \int_{t=0}^{t} (i_R(t) - i_C(t))dt \quad (8)$$

$$V_{int}(t) = \frac{Q_F(t)}{C_F(Q_F(t))} = 2\alpha Q_F(t) + 4\beta Q_F^3 + 6\gamma Q_F^5 \quad (9)$$

$V_F(t)$ is calculated using the relation: $V_F(t) = V_{int}(t) + (i_R(t) - i_C(t))\rho$.

Main text Fig. 4(b) shows the simulated transient response of the series combination of the ferroelectric capacitor and a resistor R = 50 kΩ to an AC voltage pulse V_s : -14 V →+14 V → -14 V. The simulated transient response of the same circuit with R = 200 kΩ to an AC voltage pulse V_s : -14 V →+14 V → -14 V is shown in Fig. S13. Main text Fig. 3(d) shows the comparison between the simulated $P - V_F$ curves for R = 50 kΩ and 200 kΩ.

Although the model presented here describes a single domain scenario, the negative capacitance effect is equally applicable to ferroelectric switching that occurs through nucleation and growth of domains. As long as there is a threshold and subsequent abrupt switching, a negative capacitance effect will ensue. The single domain picture tries to capture the threshold by estimating it through a double-well energy profile and as such provides the mean value of the microscopic parameters.

5.3 Estimation of ρ

The main text equation (2) can be rewritten as follows.

$$V_F(Q_F(t)) = \frac{Q_F(t)}{C_F(Q_F(t))} + \rho i_F(t) \quad (10)$$

where $i_F = dQ_F/dt$. Let us compare the dynamics of a ferroelectric capacitor for two different resistors R_1 and R_2 for the same applied voltage pulse. Let t_1 and t_2 be the time variables for these two cases, i_{F1} and i_{F2} be the corresponding currents through the ferroelectric capacitor and V_{F1} and V_{F2} be the measured ferroelectric voltages for the resistors R_1 and R_2 respectively.

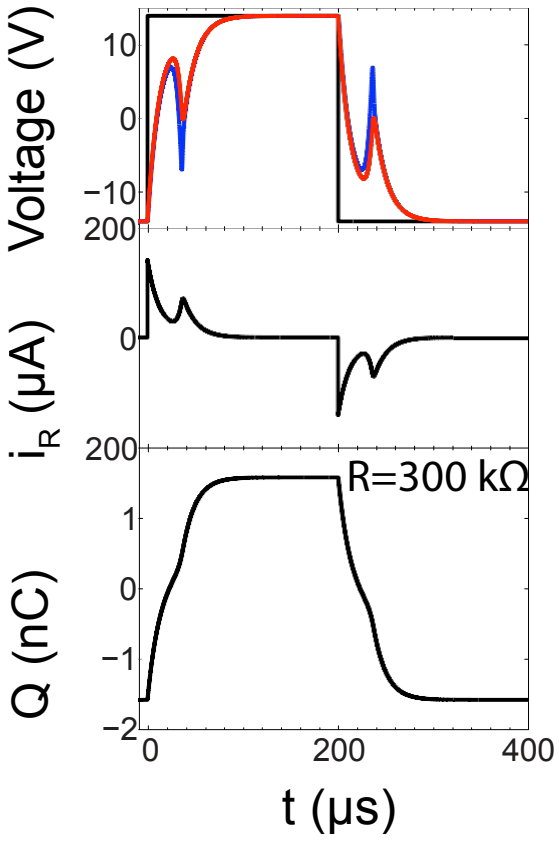

Figure S13: The simulated transient response of the series combination of the ferroelectric capacitor and a resistor R = 200 kΩ to an AC voltage pulse V_s :-14 V→+14 V→-14 V.

Hence,

$$V_{F1}(Q_{F1}(t_1)) = \frac{Q_{F1}(t_1)}{C_F(Q_{F1}(t_1))} + \rho i_{F1}(t_1) \quad (11)$$

$$V_{F2}(Q_{F2}(t_2)) = \frac{Q_{F2}(t_2)}{C_F(Q_{F2}(t_2))} + \rho i_{F2}(t_2) \quad (12)$$

Let us assume that, in the first experiment with the resistor R_1, Q_{F1} reaches a given value Q at $t_1 = \tau_1$, and in the second experiment with R_2, Q_{F2} reaches Q at $t_2 = \tau_2$ (i.e. $Q_{F1}(t_1 = \tau_1) = Q_{F2}(t_2 = \tau_2) = Q$). Hence from equation (11) and (12), the following equation for ρ can

be derived.

$$\rho(Q) \;=\; \frac{V_{F1}(t_1=\tau_1) - V_{F2}(t_2=\tau_2)}{i_{F1}(t_1=\tau_1) - i_{F2}(t_2=\tau_2)} = \frac{V_{F1}(Q) - V_{F2}(Q)}{i_{F1}(Q) - i_{F2}(Q)} \tag{13}$$

6 Dependence of ρ and the negative capacitance on the voltage amplitude

Fig. S14(a,b) show the transient response of the PZT sample to DC pulses of different applied voltage amplitudes for R=50 kΩ and 300 kΩ respectively. Before applying each of the pulses shown in Fig. S14, a large negative voltage pulse was applied to set the initial polarization along the appropriate direction. Fig. S15(a,b) show the $Q_F - V_F$ and $Q_F - i_F$ curves respectively for different applied voltage amplitudes with R= 50 kΩ and R= 300 kΩ. Fig. S15(c) shows the value of ρ calculated using equation 13 as a function of Q_F for different voltage amplitudes. Using the extracted value of ρ for a given voltage amplitude, the internal node voltage $V_{int}(Q_F(t)) = Q_F(t)/C_F(Q_F(t)) = V_F(Q_F(t)) - i_F(Q_F(t)) \times \rho$ is calculated. Fig. S16 shows the corresponding $Q_F - V_{int}$ curves. In Fig. S16, the negative capacitance state of the ferroelectric corresponds to the region under the dashed box. The average value of the negative capacitance C_{FE} is calculated using the equation: $C_{FE} = \Delta Q_F/\Delta V_{int}$, ΔQ_F and ΔV_{int} being the changes in the ferroelectric charge and the internal ferroelectric node voltage in the negative capacitance region, respectively. Fig. S17(a,b) plot the average ρ and $-C_{FE}$ respectively as functions of the applied voltage amplitude. We note in fig. S17(a) that ρ decreases monotonically with an increasing amplitude while C_{FE} remains reasonably constant. Intuitively, in a domain-mediated switching process, a larger input voltage results in more domains to nucleate at the onset. The results show that this increase in number of initial domains lead to a smaller ρ, while the negative capacitance remains fairly independent of it.

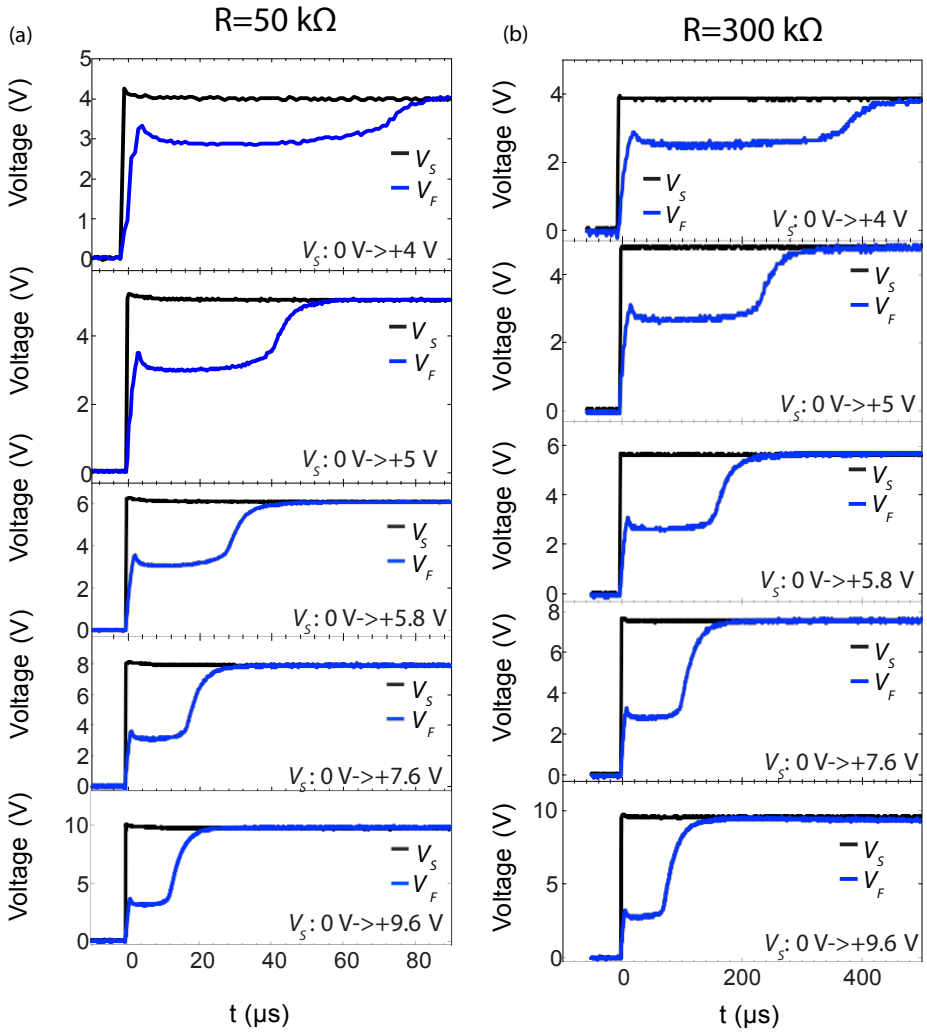

Figure S14: Transient response of the PZT sample to DC pulses of different amplitudes for R=50 kΩ (a) and 300 kΩ (b). Before applying each of the pulses, a large negative voltage pulse was applied to set the initial polarization along the appropriate direction.

7 Time duration of the negative capacitance transients

Fig. S18(a,b,c,d) show the transient response of the PZT sample to a DC pulse V_S: 0 V→ +6 V for R=2 kΩ, 25 kΩ, 50 kΩ and 300 kΩ respectively. The time duration of the negative capacitance transient t_1 is indicated in the close-up images in Fig. S18(a,b,c,d). Fig. S19(a,b)

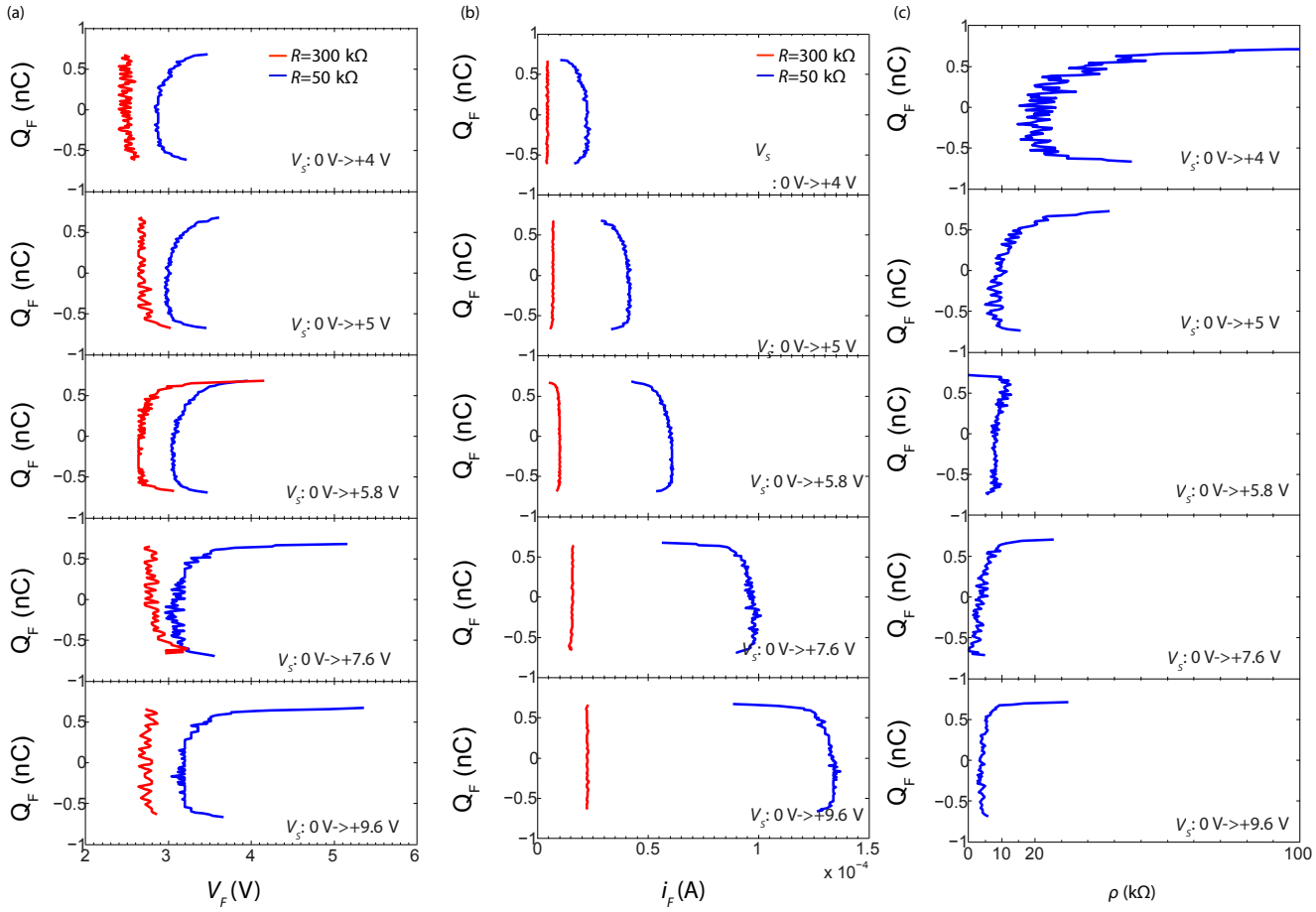

Figure S15: (a,b) $Q_F - V_F$ (a) and $Q_F - i_F$ (b) curves for different applied voltage amplitudes with R= 50 kΩ and R= 300 kΩ. (c) The value of ρ calculated using equation 13 as a function of Q_F for different voltage amplitudes.

plot t_1 as a function of R in logarithmic and linear scale respectively. In fig. S19(a,b), we observe a linear decrease of t_1 down to ~350 ns as R is decreased to 2 kΩ. Fig. S19(c) shows that the extrapolated $t_1 - R$ curve intersects the $R = 0$ line at t_1=19.9 ns.

8 Effect of the variation of the material stack

To elucidate that negative capacitance effects are not dependent upon the specific material system or thicknesses used, we show the negative capacitance transients in a different sample (a 100 nm $Pb(Zr_{0.2}Ti_{0.8})O_3$ film grown on metallic $(La_{0.7}Sr_{0.3})MnO_3$ (LSMO) (20 nm) buffered $SrTiO_3$ (001) substrate). The heterostructure was grown using the same pulsed laser deposition technique and 20 μm × 20 μm gold electrodes were fabricated using standard lithographic techniques. Fig. S20(a) shows the hysteresis loop of the sample measured using a typical Sawyer-Tower type setup. The remnant polarization of the sample is ∼0.78 C/m^2 and the coercive voltage is ∼±2V. Fig. S20(b) shows the dielectric characterization of the sample. Fig. S20(c,d) show that the transient response of the 100 nm PZT with a series resistor R = 300 kΩ to AC voltage pulses V_s :-1.8 V→+1.8 V→-1.8 V and V_s :-3 V→+3 V→-3 V respectively. We note in fig. S20(c) that no negative capacitance transients are observed since the applied voltage is smaller that coercive voltage. On the other hand, in fig. S20(d), the applied voltage is larger than the coercive voltage and as such the negative capacitance transients are observed. This indicates that as long as a single crystalline ferroelectric with abrupt switching behavior can be grown, a negative capacitance effect is expected.

References and Notes

1. C. B. Sawyer, C. H. Tower, *Phys. Rev.* **35**, 269 (1930).

2. K. Rabe, C. Ahn, J. Triscone, *Physics of Ferroelectrics: A Modern Perspective*, Topics in applied physics (Springer).

3. D. V. Taylor, D. Damjanovic, *Journal of Applied Physics* **82** (1997).

4. R. E. Eitel, T. R. Shrout, C. A. Randall, *Journal of Applied Physics* **99**, (2006).

5. C. Pawlaczyk, *et al.*, *Integrated Ferroelectrics* **9**, 293 (1995).

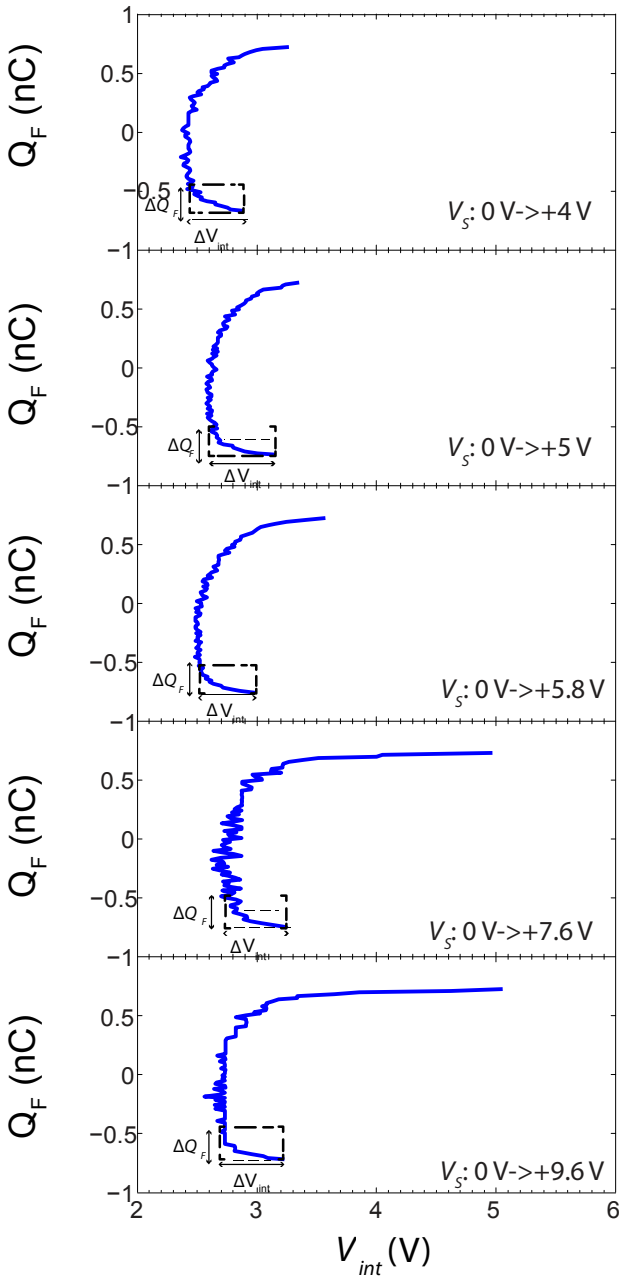

Figure S16: $Q_F - V_{int}$ curves for different voltage pulses. The negative capacitance state of the ferroelectric corresponds to the region under the dashed box.

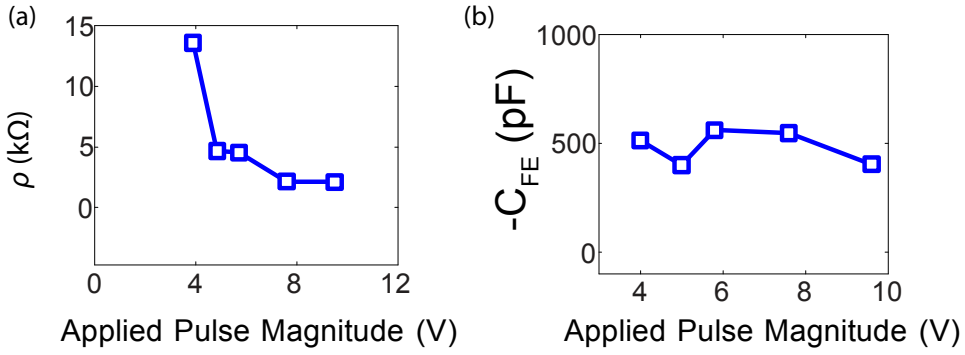

Figure S17: Average ρ (a) and $-C_{FE}$ (b) as functions of the applied voltage magnitude.

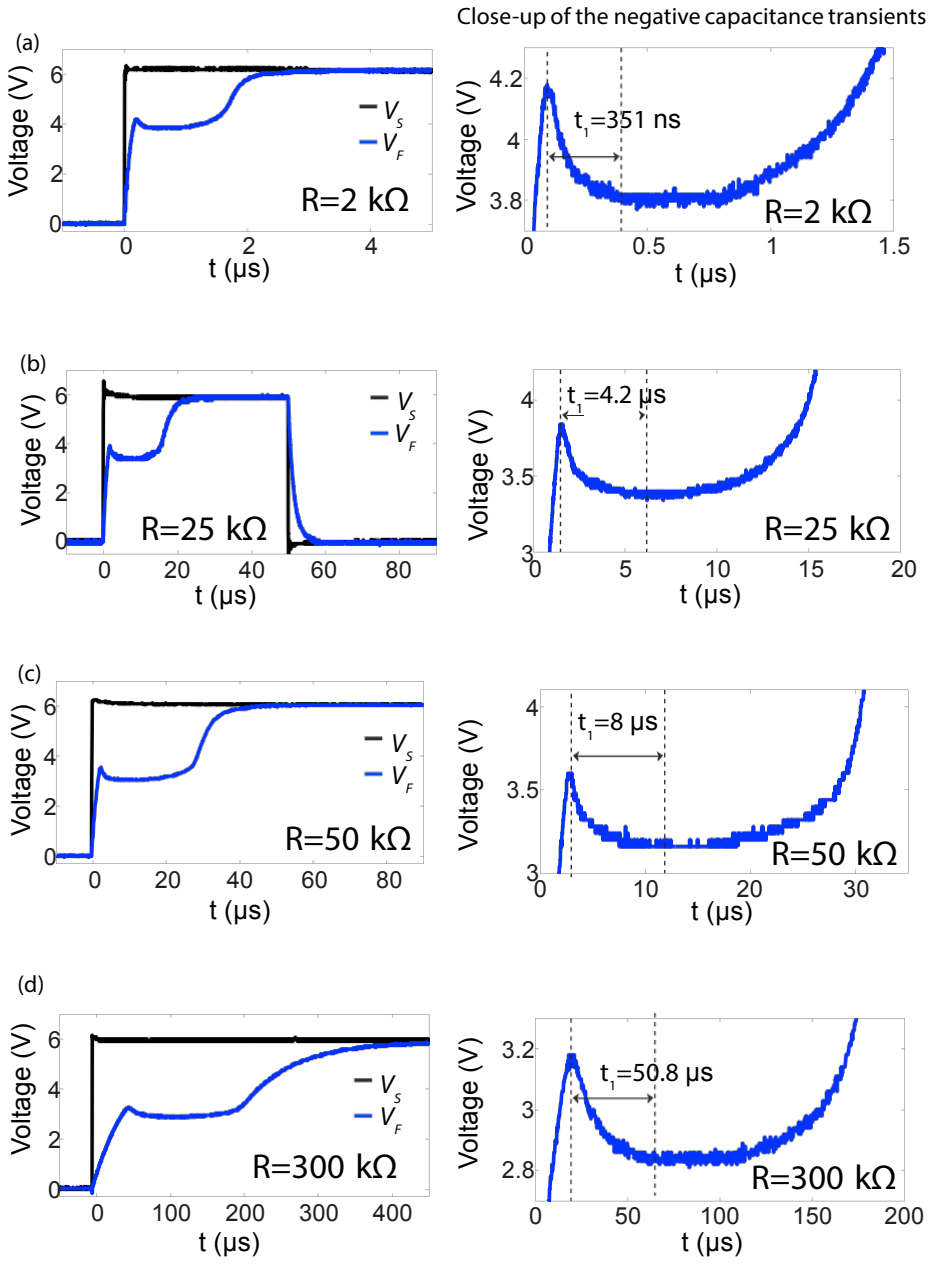

Figure S18: Transient response of the PZT sample to a DC pulse V_S: 0 V→ +6 V for R=2 kΩ (a), 25 kΩ (b), 50 kΩ (c) and 300 kΩ (d). Before applying each of the pulses, a large negative voltage pulse was applied to set the initial polarization in the appropriate direction.

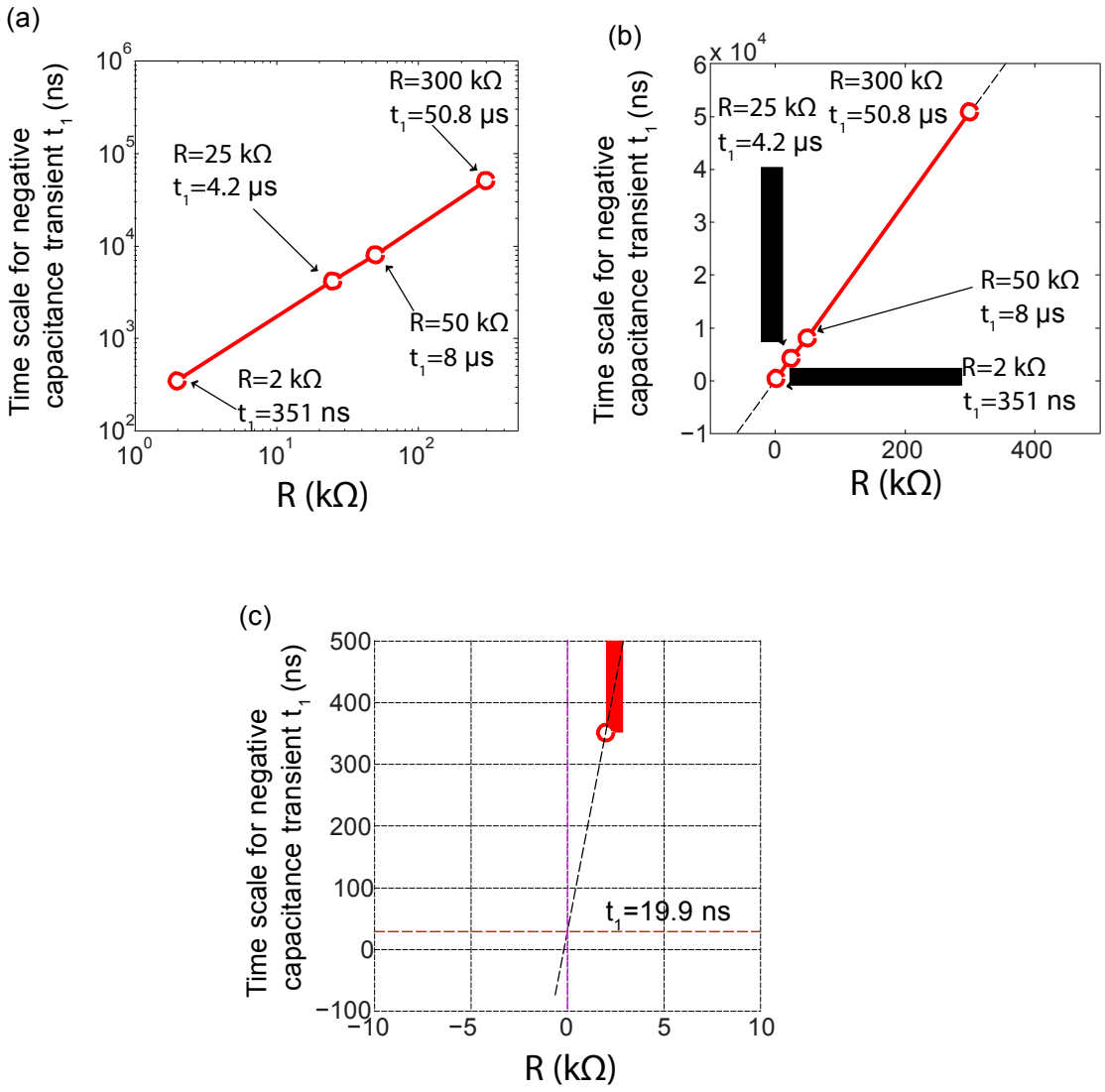

Figure S19: (a,b) The time duration of the negative capacitance transient t_1 as a function of R in logarithmic (a) and linear scale (b). (c) Extrapolation of t_1 vs. R curve to $R = 0$.

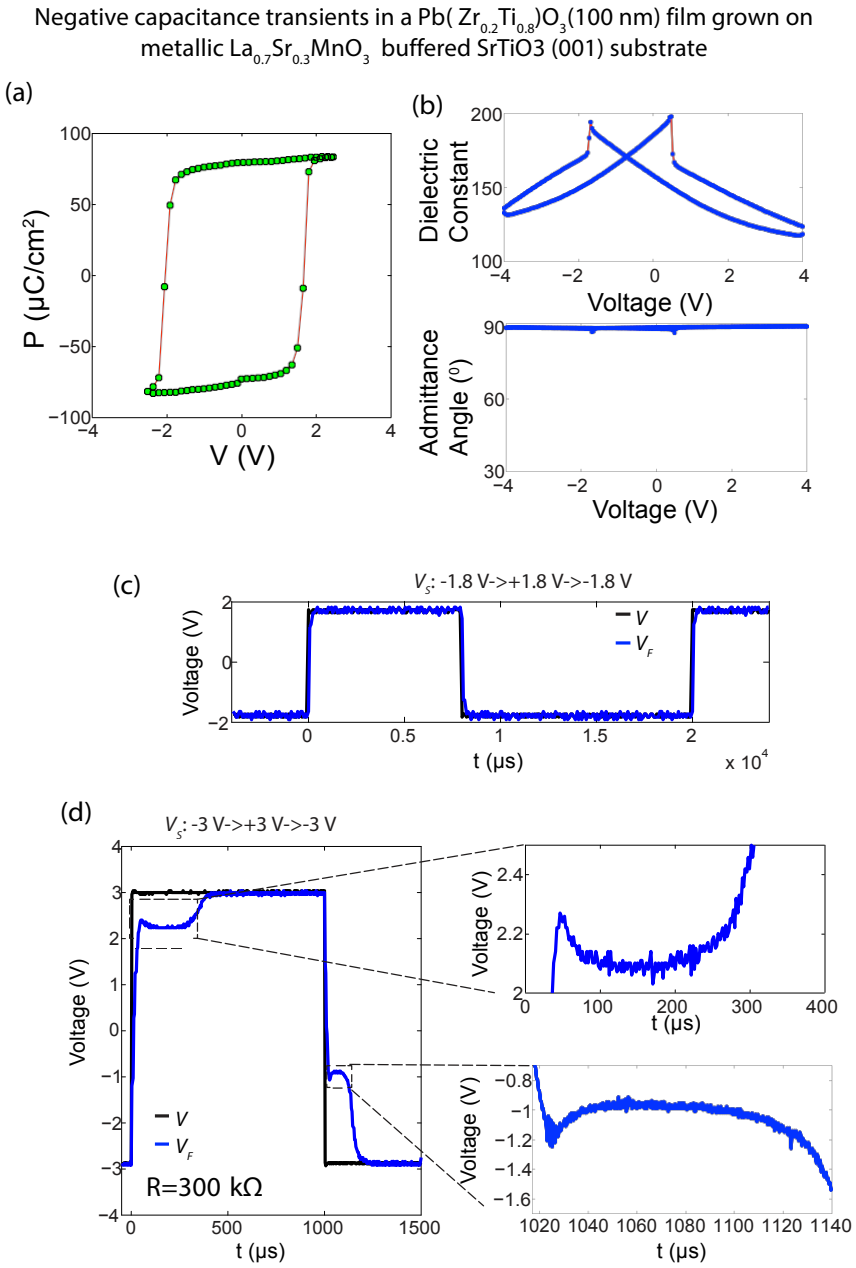

Figure S20: (a) The polarization (P)-voltage (V) hysteresis curve of a PZT (100 nm) film grown on LSMO (20 nm) buffered STO (001) substrate. The hysteresis curve is measured using a Sawyer-Tower type setup. (b) The dielectric constant-voltage and the admittance angle-voltage characteristics of the PZT(100nm)/LSMO(20 nm) on STO (001) sample at 100 kHz. (c,d) Transient response of the series combination of the ferroelectric capacitor and a resistor R = 300 kΩ to AC voltage pulses V_s :-1.8 V→+1.8 V→-1.8 V (c) and V_s :-3V→+3 V→-3 V (d).